Materials Chemistry and Physics 175 (2016) 81–91

Contents lists available at ScienceDirect

Materials Chemistry and Physics

journal homepage: www.elsevier.com/locate/matchemphys

Magnetism and structure of nanocomposites made from magnetite and vegetable oil based polymeric matrices

Cintia Meiorin [a, c, **], Oscar Moscoso Londoño [a], Diego Muraca [a, *], Leandro M. Socolovsky [b], Kleber R. Pirota [a], Mirta I. Aranguren [c], Marcelo Knobel [d], Mirna A. Mosiewicki [c]

[a] Laboratorio de Materiais e Baixas Temperaturas (LMBT), Instituto de Fisica Gleb Wataghin, Universidade Estadual de Campinas, CEP 13083-859 Campinas-SP, Brasil
[b] Laboratorio de Sólidos Amorfos (LSA), INTECIN, Facultad de Ingeniería, Universidad de Buenos Aires - CONICET, C1063ACV Buenos Aires, Argentina
[c] Instituto de Investigaciones en Ciencia y Tecnología de Materiales (INTEMA), Facultad de Ingeniería, Universidad Nacional de Mar del Plata – CONICET, Mar Del Plata, Argentina
[d] Laboratório Nacional de Nanotecnologia (LNNano/CNPEM), Rua Giuseppe Máximo Scolfaro 10000, 13083-100, Campinas-SP, Brazil

HIGHLIGHTS

- Interparticle interactions are controlled by adjusting the matrix components.
- Particle aggregation into the matrices was monitored by the Fractal Aggregate Model.
- Magnetization results were analyzed by the Interacting Superparamagnetic Model.
- Bio-based magnetic nanocomposites are promising materials in industrial applications.

GRAPHICAL ABSTRACT

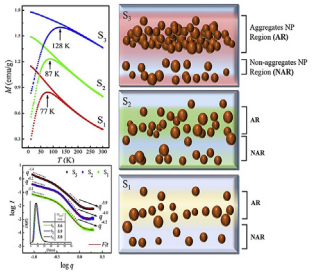

ARTICLE INFO

Article history:
Received 21 August 2015
Received in revised form
17 February 2016
Accepted 25 February 2016
Available online 22 March 2016

Keywords:
Magnetic materials
Magnetometer
Polymer
Nanostructures

ABSTRACT

The aim of this work is to study the influence of the polymeric matrix composition on particle aggregation, magnetic interparticle interactions and nanoparticle surface effects, which affect the magnetic and structural properties of different ultra-diluted magnetite nanocomposites (MNCPs). Bio-based matrices were selected as a possible response to the increasing demand for renewable materials. To investigate the influence of different bio-based polymeric matrices on the magnetic behavior, three different bio-based polymers were used to prepare MNCPs with 1 wt.% of magnetite nanoparticles (MNPs). One of them was prepared using a tung oil (TO)/styrene (St) weight ratio of 70/30, a second one was prepared by replacing the styrene with methylester (green comonomer obtained from tung oil, ME, 70TO/30ME) and a third one that incorporated a green modifier, acrylated epoxidized soybean oil (AESO), using a tung oil/AESO weight ratio of 90/10. Structural features as nanoparticle aggregation state, nanoparticle and cluster sizes, and fractal dimension were studied and determined from small-angle X-ray Scattering (SAXS). The experimental SAXS data were analyzed by means of fractal aggregate model. Results indicate differences in nanoparticle arrangement depending of the containing matrix. The magnetic characterization of these materials indicates that the matrix strongly affects the physical and chemical properties of the MNCPs. All samples display superparamagnetic behavior at room

* Corresponding author.
** Corresponding author.
E-mail addresses: cintia.meiorin@fi.mdp.edu.ar (C. Meiorin), dmuraca@ifi.unicamp.br (D. Muraca).

http://dx.doi.org/10.1016/j.matchemphys.2016.02.071

temperature, but the blocking temperature varies from 75 K (tung oil/styrene with 1 wt.% MNPs) to 126 K (tung oil/AESO 1 wt.% MNPs). Furthermore, the temperature dependence of the coercive field changes for all samples, suggesting a strong influence of the polymer properties on the magnetic properties of the MNCPs.

1. Introduction

The production of polymeric bio-based nanocomposites has become an important area of research and development due to the potential applications of these materials in different scientific and industrial fields [1,2] as well as biotechnology and biomedicine [3]. Particularly, in pharmaceutical applications, it is possible to control the drug delivery by using polymeric materials loaded with magnetic nanoparticles which are activated with external magnetic fields [4–6]. When a magnetic field is applied over a magnetic nanocomposite, drugs previously loaded into the MNCP can be released. On the other hand, the bio-based nanocomposites have numerous applications in the aircraft, automobile and machine industries, where they can be used for noise reduction and prevention of vibration induced fatigue failure [7].

In order to develop technological applications, cheap and easy-to-obtain magnetic nanocomposites are preferable. Specifically, the development of polymeric composites obtained from renewable raw materials additionally presents several environmental advantages [8,9]. These bio-based nanocomposites can be described as bio-based matrices reinforced with magnetic nanoparticles [1,3,10]. Even though in the recent years the production of these kind of materials has grown considerably, few authors use vegetable oils as raw materials to prepare nanocomposites using magnetite nanoparticles as fillers [11–13].

Physico-chemical properties of this class of MNCPs are regulated by several factors, such as type of magnetic particles, size, polydispersity, coating and concentration within the matrix, as well as the chemical nature of the containing matrix, among others. In the last few years, the ability to control the aforementioned aspects has led to a number of potential applications. Some of these are centered on the fact that the magnetic nanoparticles can be thermally activated by an alternating magnetic field, producing a release of heat, which under specific conditions, can be used to change the mechanical properties of the MNCPs, e. g. stress for MNCPs for shape memory or actuators, diffusion coefficient for MNCPs for drug delivery, etc [14–21]. Such release of heat also can be exploited for hyperthermia treatment of cancer [22–25], in this sense and according to latest reports, increase in magnetic interactions between nanoparticles amplifies the specific absorption rate (SAR) [22,23], which is an important parameter to take in account for hyperthermia treatments. Usually, to obtain polymer-magnetic nanocomposites with higher interparticle interactions is necessary to increase the percentage of magnetic nanoparticles with respect to the total volume of the composite. However, for *in-vivo* applications, such as magnetic hyperthermia, an increase in the amount of magnetic nanoparticles may not be viable. Thus, it is necessary to find alternatives that would allow enhancing the magnetic interparticle interactions without increasing the nanoparticle concentration. Concerning this we explore a way to increase the interparticle interactions by adjusting the matrix components, but keeping the nanoparticle concentration constant.

In a previous work [12], superparamagnetic polymer nanocomposites were prepared from the incorporation of magnetite nanoparticles (1 and 9 wt.%) into a matrix composed by tung oil and styrene using a weight ratio of 50/50. We studied the morphology, dynamic-mechanical and mechanical properties of these MNCPs, as well as basic magnetic properties, from which we concluded that they were significantly affected by the variation of the concentration of the MNPs.

From previous results, we inferred that it would be necessary to consider systems with low concentration of MNPs (1 wt.%) in other matrices, in order to study how the interaction among the MNPs and the matrices affects the thermal, dynamic-mechanical, mechanical and magnetic properties, among others. Considering this objective, three novel matrices with 1 wt.% of MNPs concentration were prepared. The same matrices without MNPs were also prepared and previously characterized [26]. The first one was prepared using a tung oil/styrene weight ratio of 70/30 (called S_1). A second one (called S_2) was prepared replacing the styrene monomer for methylester (ME), which is a green monomer (obtained by transesterification of the tung oil with methanol) in the same weight ratio (70/30). Finally, a last one (called S_3), consisted in the incorporation of a green modifier, a commercial acrylated epoxidized soybean oil (AESO), using a tung oil/AESO weight ratio of 90/10.

Small angle X-ray scattering method was used to investigate the structure of the MNPs within the non-magnetic matrix. Cluster formation was followed by means of the fractal aggregate model. Magnetic experimental results were analyzed by means of the interacting superparamagnetic model (ISP) [27] that takes into account magnetic interactions of dipolar origin. This model gives an indirect analysis of MNP aggregations in the MNCPs, obtaining an excellent agreement for magnetic nanocomposites with low MNPs concentration (1 wt.%). When the ISP model is used in magnetic nanocomposites with concentrations higher than 1 wt.% spurious results appear as a consequence of stronger–dipolar interactions among MNPs, possibly due to a more compact agglomeration of the nanoparticles.

The aim of this work is to study more exhaustively the magnetic and structural properties of bio-based nanocomposites synthesized from different bio-based polymeric compounds, which were used as support matrix for magnetite nanoparticles (1 wt.%). Magnetic results of the three samples synthesized for this work are compared with those already reported for a sample made from tung oil and styrene with 1 wt.% MNPs [12].

2. Experimental procedures

2.1. Materials

The vegetable oil used, tung oil (TO), is a triester of glycerol and fatty acids, being the major fatty acid constituent α-elaeostearic acid (84 wt.%). The monomers used in the copolymerization with tung oil were: styrene (St) 99.95% pure supplied by Cicarelli and a monomer synthesized in our laboratory, methylester from tung oil (ME) obtained by transesterification reaction [26]. The modifier was a commercial acrylated epoxidized soybean oil (AESO) purchased from Sigma–Aldrich. Boron trifluoride diethyl etherate ($BF_3.OEt_2$) with 46–51% BF_3, obtained from Sigma–Aldrich was the initiator of the cationic reaction and was modified with

tetrahydrofurane 99% pure, (THF) from Cicarelli.

For the magnetic nanoparticles the following reagents (Sigma–Aldrich) were used as received: ferric chloride hexahydrate ($FeCl_3 \cdot 6H_2O$), ferrous chloride tetrahydrate ($FeCl_2.4H_2O$), ammonium hydroxide (28–30% NH_3) and oleic acid (Aldrich). N-heptane was used as solvent (P.A. grade).

2.2. Methods and techniques

2.2.1. Magnetite nanoparticles (MNPs) preparation

Magnetite nanoparticles were prepared by a co-precipitation method from an aqueous Fe^{3+}/Fe^{2+} solution using excess of concentrated ammonium hydroxide. Specifically, 0.09 mol of $FeCl_3 \cdot 6H_2O$ and 0.06 mol of $FeCl_2.4H_2O$ were dissolved in 50 mL of distilled water and heated at 70 °C. After that, 40 mL of NH_4OH were added and the formation of a black precipitated was immediately observed [28].

The obtained nanoparticles were subsequently coated with oleic acid by adding 0.02 mol of oleic acid and the suspension heated to 80 °C for 30 min. The obtained oleic acid coated magnetite nanoparticles were washed with distilled water and separated by centrifugation several times until neutral pH was obtained. Finally, they were dispersed in n-heptane to form a stable ferrofluid and stored until future use.

2.2.2. Preparation of bio-based compounds and magnetic nanocomposites (MNCPs)

For the synthesis of the copolymers of tung oil (TO) with styrene (St) and with methyl ester of tung oil (ME) used in the preparation of the nanocomposites (MNCP), a weight ratio of 70/30 (TO/comonomer) was selected (sample S_1 and S_2, respectively). In the case of the MNCP prepared with acrylated epoxidized soybean oil (AESO) the weight ratio (TO/modifier) was selected as 90/10 (sample S_3). In all cases, the mixture was stirred for few minutes before proceeding to the addition of 3 wt.% of modified initiator ($BF_3.OEt_2$ plus 5 wt.% of THF). As it was reported [29,30], due to the poor miscibility of the catalyst in the oils, it must be modified to obtain a homogeneous initial solution. A selected percent of oleic acid-coated magnetite nanoparticles (1 wt. %) was added to the original mixture. Then, this mixture was sonicated in an ultrasonic device to obtain a good dispersion of magnetite nanoparticles and finally, poured into glass plates of 13 mm × 18 mm separated by a rubber cord of 1 mm of thickness and kept closed with metal clamps. The reactants were heated first at 25 °C for 12 h, then at 60 °C for 12 h and finally at 100 °C for 24 h. After curing, the samples were conditioned at room temperature, in a normally illuminated area, inside a desiccator containing silica gel to maintain a dry atmosphere.

Throughout this manuscript the following nomenclature for samples will be used: bio-based polymeric compounds without magnetic nanoparticles as S_1, S_2 and S_3 and the corresponding magnetic nanocomposites with 1wt. % of MNPs as M_1, M_2 and M_3, respectively. Magnetic nanocomposite 50TO/50St with 1wt.% of MNP (comparative sample for magnetic analysis) is called M_X.

2.2.3. Thermogravimetric analysis (TGA)

Thermogravimetric analysis of MNCPs was performed using a TGA-50 SHIMADZU at a heating rate of 10 °C/min under air atmosphere. Samples were dried in a vacuum oven until constant weight, before performing the analysis.

2.2.4. Dynamical-mechanical tests (DMA)

A Perkin Elmer dynamic mechanical analyzer (DMA 7) was used to determine the dynamic mechanical behavior of the samples using the tensile fixture and temperature scan mode under nitrogen atmosphere, with dynamic and static stresses of 50 and 100 kPa, respectively. The sample dimensions were 20 × 5 × 0.5 mm3. At least three tests for each sample were carried out in order to ensure reproducibility of the results. The frequency of the forced oscillations was fixed at 1 Hz and the heating rate was of 10 °C/min.

2.2.5. Mechanical tests: microtensile testing

Microtensile testing were performed at 18 °C on tensile specimens of 5 mm × 35 mm × 1 mm cut from the molded plaques, using a universal testing machine (INSTRON 8501), in accordance with ASTM D 1708-93 at a crosshead speed of 5 mm/min. Young's modulus (E), ultimate stress (σ_u) and elongation at break (ε_u) were determined from the average values of at least four replicates for each sample.

2.2.6. Scanning electron microscopy (SEM)

The scanning electron microscopy images were taken at the LNNano of National Nanotechnology Laboratory (CNPEM, Campinas, Brazil). The samples were analyzed with a FEI Inspect F-50 Field Emission Scanning Electron Microscope (FE-SEM) equipped with energy dispersive X-ray spectroscopy (EDS) attachment for elemental analysis. Since the samples are non-conductive, they were previously coated with a gold layer of about 16 nm in thickness.

2.2.7. Small-angle X-ray scattering (SAXS)

Small-angle X-ray Scattering (SAXS) experiments were performed on SAXS2 beamline at the Brazilian Synchrotron Light Laboratory (LNLS), Centro Nacional de Pesquisa em Energia e Materiais (CNPEM), Campinas, Brazil). The measurements were carried out at room temperature. The scattering intensity was measured as function of momentum transfer vector q ($q = 4\pi \sin\theta/\lambda$), in a range from 0.08 to 2.0 nm^{-1}, being θ is the scattering angle and with a wavelength of $\lambda = 1.822$ Å. Data treatment was performed using the software SASFit (0.94.6 version). All SAXS experiments were conducted under controlled environmental conditions (20 °C and 45 ± 5% relative humidity).

2.2.8. Static magnetic properties

Magnetic properties of the nanocomposites were studied using a SQUID magnetometer (Quantum Design, MPMS XL). The magnetic field dependence of magnetization was measured with field up 1600 kA/m (±2T) at various temperatures. Magnetization versus temperature curves were performed in zero field cooled (ZFC) and field cooled (FC) modes. In the ZFC mode, the sample was cooled under a zero magnetic field. Then, a static magnetic field of 4 kA/m was applied and the magnetization was measured as the temperature was increased to 300 K. In the FC mode, the sample was cooled in the presence of a magnetic field of 4 kA/m and the magnetization was measured during warming under the same field.

3. Results and discussion

3.1. Thermogravimetric analysis (TGA)

TGA analysis of the materials with and without 1 wt.% of MNPs was performed to evaluate the effect of the addition of magnetic nanoparticles on the thermal degradation of the composites.

Fig. 1 shows the TGA curves of the magnetic (M_1, M_2 and M_3) and non-magnetic (S_1, S_2 and S_3) samples. MNCPs loaded with 1 wt.% of MNPs have a similar weight loss than the original matrices in the temperature range 420–620 K. The most important differences with respect to the degradation of the original matrices, are

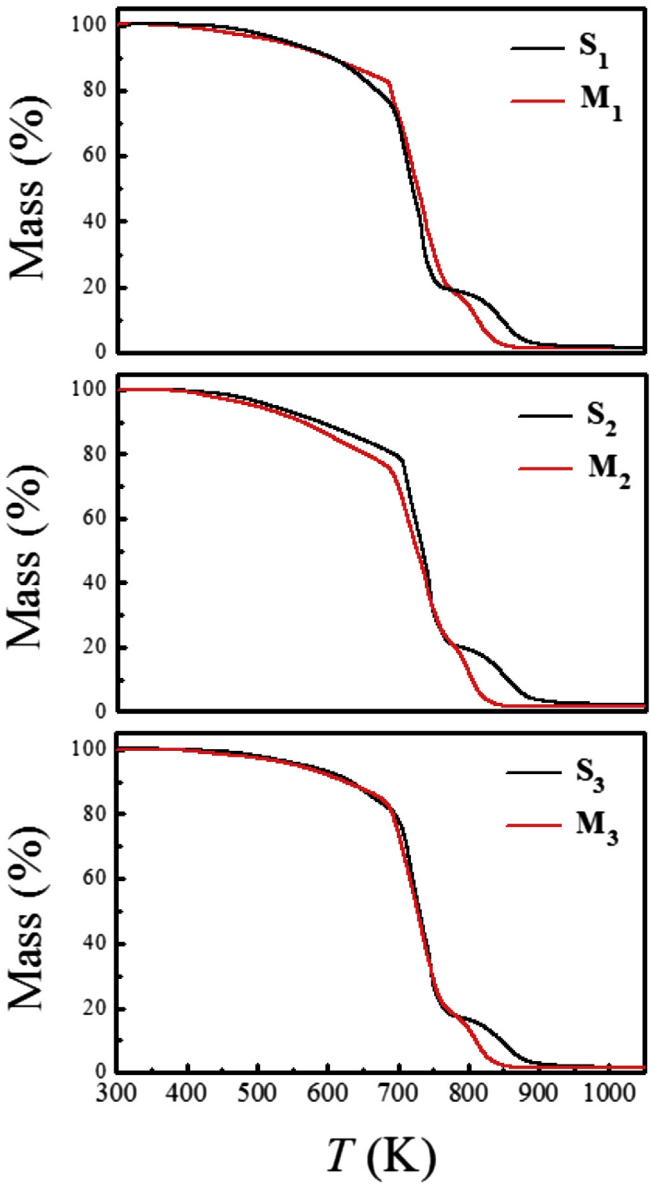

Fig. 1. Thermogravimetric curves for the samples of S_1, S_2, S_3, M_1, M_2 and M_3.

observed in the range of 770–920 K, where all the curves with 1 wt.% of MNP show a larger weight loss. This behavior could be attributed to the fact that the polymer layer on the surface of the magnetic nanoparticles can present a physical conformation quite dissimilar in comparison to the well-developed polymeric structure of the bulk polymer. This last effect was also reported by authors that have worked with nanocomposites of quitosan and magnetite where the reduction in the thermal stability of the matrices was attributed to the fact that the chitosan deposited on the surface of the magnetic particles has lower crystallinity and lower rigid molecular structure compared to the free chitosan, requiring less energy to achieve its thermal degradation [31–34].

In all cases, the sensitivity of the equipment is not enough to detect significant changes above 920 K between the neat polymer and the MNCPs at the concentrations of MNP used (1 wt.%), and thus, TGA results could not be used to confirm the magnetite content in the MNCPs.

3.2. Dynamical-mechanical tests (DMA)

Fig. 2 shows the variation in tan δ (damping or loss factor) and the storage modulus (E′) as a function of temperature in samples M_1 and S_1. The same tendency has been previously reported [12] for M_X sample: two peaks were observed in the loss factor curve, while the main maximum of the curve, (related to the glass transition temperature, Tg, of the sample) was shifted toward higher temperatures with the addition of MNPs (increase of about 40 K with respect to the matrix). The reason for this outstanding increase in Tg can be explained as the result of the incorporation of magnetic nanoparticles of high rigidity, together with the good interaction at the interfaces between polymer matrix and coated magnetic nanoparticles.

In addition, the considerable changes in the shape of the curves are attributed to the heterogeneity of the system, where some regions in the sample correspond to the bulk polymer, and other regions are influenced by interactions with the magnetic nanoparticles. On the other hand, the tan δ factor >0.3 over a wide temperature range, indicates good damping capacity of the material [35].

Regarding to the storage modulus, the MNPs addition also increases this property over the range of temperatures tested, but with greater effect at temperatures above the glass transition temperature of the copolymer without magnetic nanoparticles.

Fig. 3 shows the dynamical–mechanical curves as functions of temperature for samples S_2 and M_2. As it was observed for other copolymers, the incorporation of MNPs causes a shift of the maximum in tan δ curve at higher temperatures (283 K–310 K). In this particular case, a small shoulder also appears between 250 K and 280 K, which could be attributed to the relaxations of less reactive components of the methyl ester of tung oil. This sample shows a small reduction in the vitreous and rubbery modulus (low and high temperatures) with the addition of MNPs. However, the drop in the storage modulus (transition region) occurs at higher temperatures in comparison with the neat copolymer TO/ME, and thus, the room temperature storage modulus increases with the MNP addition. As it was previously mentioned, the addition of MNPs modifies the structure of the material, which leads to the observed changes in the storage modulus.

Fig. 4 shows the behavior of the samples S_3 and M_3, with Tg

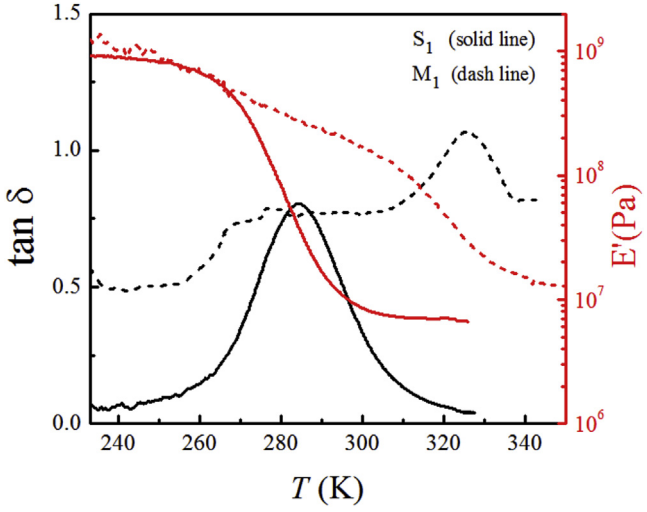

Fig. 2. Tan δ vs temperature curves for the S_1 and M_1 samples.

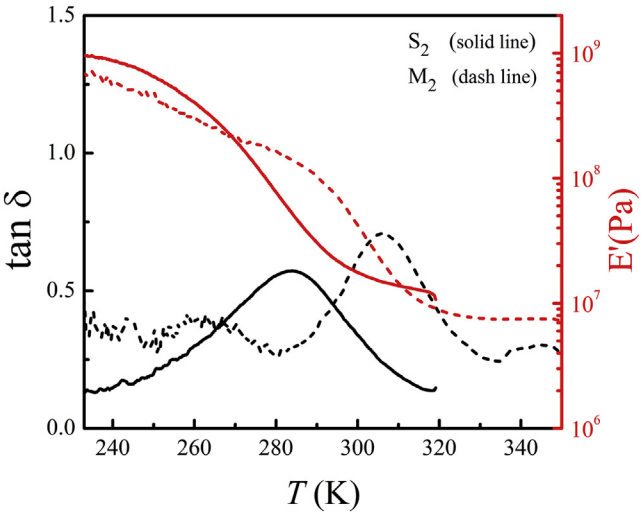

Fig. 3. Tan δ vs temperature curves for the S_2 and M_2 samples.

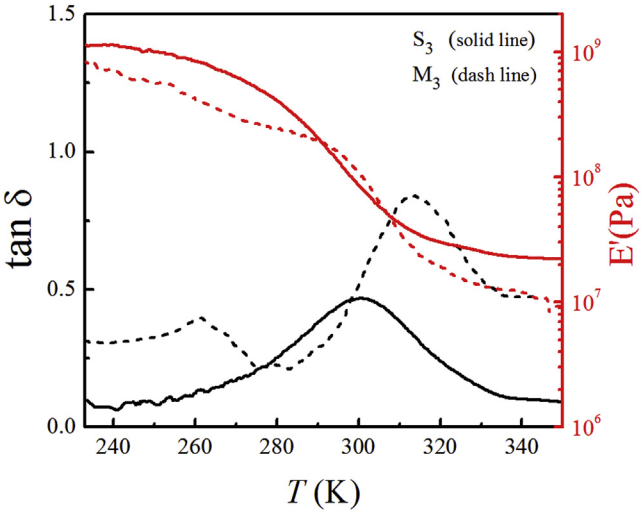

Fig. 4. Tan δ vs temperature curves for the S_3 and M_3 samples.

increasing from 300 K to 313 K and also showing that the storage modulus is reduced in the whole temperature range analyzed. The effect is similar to that observed in the nanocomposite synthesized with ME, with the modulus reduction resulting from the less effective network formation, and the Tg increasing because of the effect of the addition of rigid magnetic nanoparticles with good interfacial adhesion towards the matrix [36,37]. For MNCPs, as well as for matrix without MNPs, is noted that tan $\delta > 0.3$ at temperatures above (but close to) ambient temperature. Thus, all MNCPs maintained good damping properties over a range of temperature wider than the unfilled materials.

3.3. Mechanical tests

Mechanical properties obtained from tensile tests are summarized on Table 1. It can be noticed that the addition of 1 wt.% of MNPs within the S_1 matrix increases the Young's modulus of the material (M_1). Also, there is a significant increase in other mechanical properties (σ_u, ε_u) thus, MNPs act as reinforcement for this matrix. As already discussed, the addition of the MNPs produces a large shift of the Tg of the TO/St sample, which results in the

Table 1
Mechanical properties of the copolymers based on TO/St, TO/ME and TO/AESO with 1 wt.%. of MNP.

Sample	E (MPa)	σ_u (MPa)	ε_u (%)
S_1	4.89 ± 0.55	0.52 ± 0.24	10.55 ± 3.55
M_1	12.49 ± 4.04	1.64 ± 0.20	17.52 ± 4.93
S_2	5.87 ± 0.31	0.49 ± 0.09	8.04 ± 1.41
M_2	4.26 ± 0.40	0.32 ± 0.12	8.76 ± 2.26
S_3	10.28 ± 2.74	0.54 ± 0.11	8.90 ± 1.16
M_3	10.72 ± 0.99	1.14 ± 0.07	12.78 ± 1.98

measurement of its mechanical properties at a temperature below its Tg (test temperature = 291 K < Tg of the material); consequently a much higher modulus than that of the neat polymer is measured.

On the other hand, a decrease in the modulus and strength of the S_2 material is registered when 1wt.% of MNPs is added. In this case, the shift in Tg is not large enough to compensate for the observed reduced networking (already discussed in the DMA section). Regarding the AESO modified TO network, the modulus is not much affected by the presence of the modifier, but the tensile strength and elongation at break are largely improved. The increase in strength, compared to the unreinforced matrix, could be related to the good interaction of the oleic acid coated magnetite nanoparticles with the matrix with high content of tung oil.

Summarizing, it is clear that the MNPs are not inert fillers in all the MNCPs, since according to the results of DMA and TGA, the presence of the magnetic nanoparticles would affect the structure of the polymer network and the spatial arrangement of MNPs inside the matrices.

3.4. Morphology

Fig. 5 shows the surface morphology of the MNCPs with 1wt.% of MNPs. As it can be observed, different morphologies are noticed for the matrices under study. This can be attributed to the heterogeneity of the systems; some regions in the polymer correspond to the bulk polymer, essentially unaffected by the incorporation of the MNPs, while others regions are affected by interactions with MNPs. Inhomogeneities appear in the materials with the addition of MNPs. In concordance with results discussed above, MNCPs present different degrees of dispersion and aggregation. Electron dispersive spectroscopy, EDS (spectrum not show here), evidenced the presence of a Fe_3O_4 phase in low concentrations in all the MNCPs under study.

3.5. SAXS analysis

From the DMA analysis it became clear that the differences in the aggregation state are related with the interaction among the surfactant layer around the particles (OA) and the different compounds of the bio-based polymeric matrices. In this vein, we used SAXS technique to study the nanostructure of these three magnetic composites and the aggregation state of the MNPs within the matrices.

The experimental scattering profiles (symbols), shown in Fig. 6, are slightly different, however all spectra display a smooth decreasing q-behavior. In low-q region, all spectra display different power law behaviors, with values of exponent of −1.1, −1.2 and −1.4 for samples M_1, M_2 and M_3, respectively. These values are different from the Guinier law (behavior expected for ultra-dispersed systems) and arise from the scattering interference between the neighboring iron oxide nanoparticles, indicating and confirming that magnetic nanoparticle aggregation has occurred [38,39]. On the other hand, in the high-q region the slope is close

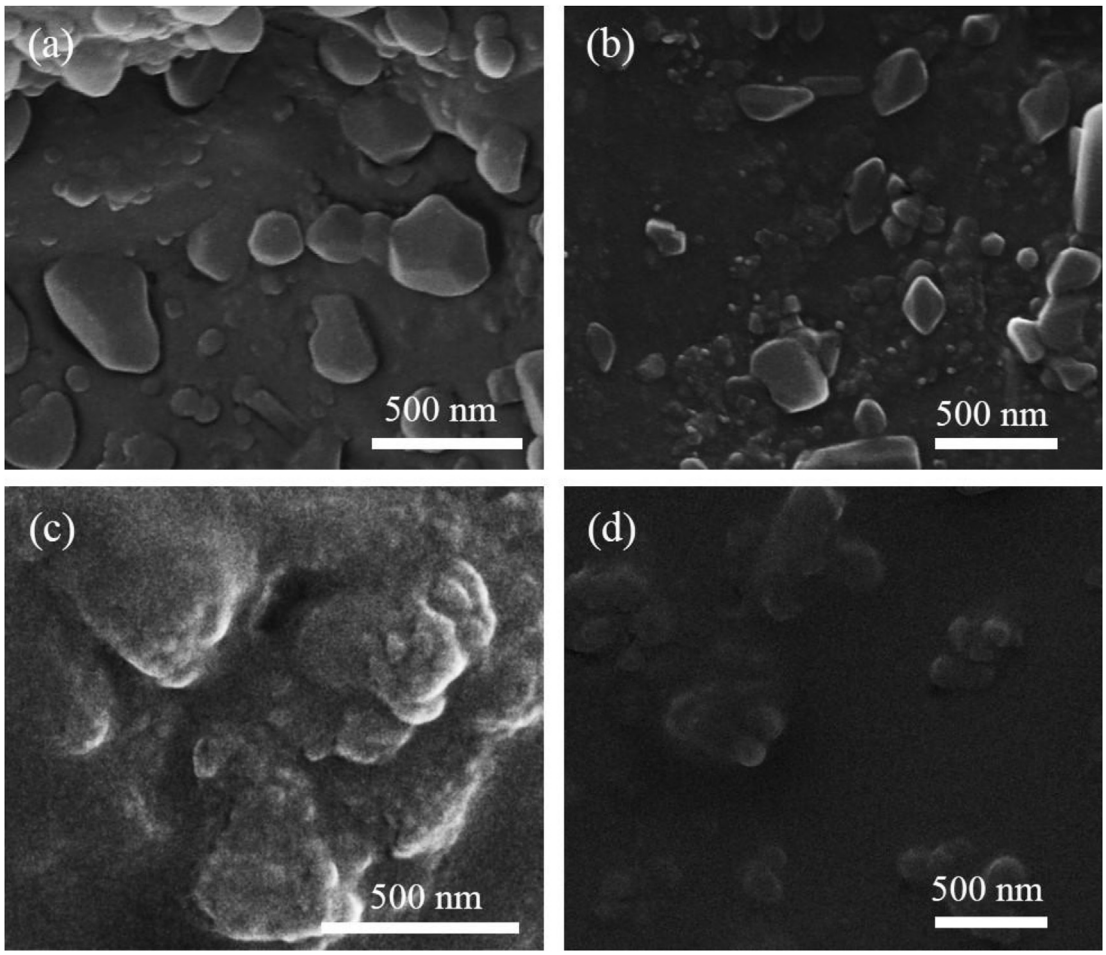

Fig. 5. SEM micrographs of the MNCP's surface. (a) M_X, (b) M_1, (c) M_2 and (d) M_3.

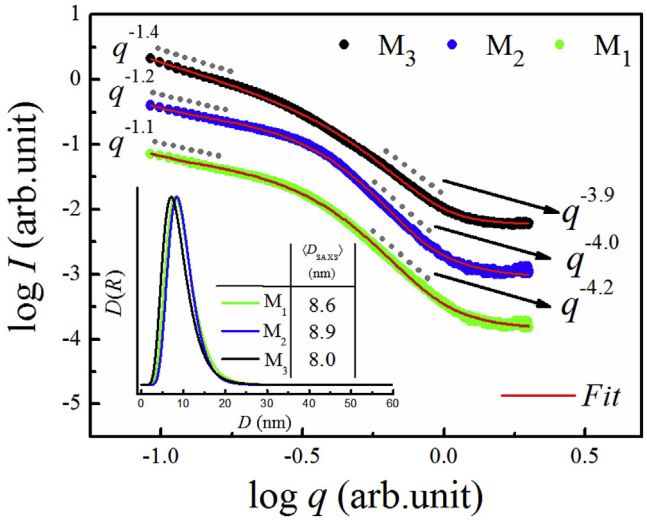

Fig. 6. Double-logarithmic representation of SAXS spectra of samples M_1, M_2 and M_3. Red continuous lines are the fitted curves using the model explained in the text. The insets show the resulting size distribution of the primary particles.

to −4 for the three samples, characteristic of Porod scattering from the smooth surface of the elementary particles. The shoulder in the central region would correspond to interparticle scattering from magnetite nanoparticles [40].

In order to perform a quantitative analysis, in addition to analyze these results with an appropriate procedure, we adopted an expression suggested by Chen and Teixeira [41]. Briefly, this procedure considers the use of a structure factor $S(q)$ of fractal aggregates composed of primary particles of radius r_0. This structure factor is given by:

$$S(q) = 1 + \frac{D_F \Gamma(D_F - 1)}{(qr_0)^{D_F}} \frac{\sin\left[(D_F - 1)\tan^{-1}(q\xi)\right]}{\left[1 + 1/(q\xi)^2\right]^{(D_F-1)/2}} \quad (1)$$

In previous equation $\Gamma(D_F - 1)$ is the gamma function and D_F is the fractal dimension. The parameter ξ is the finite cluster size that appears in the $h(r_0, \xi)$ cut-off function. Such function describes the perimeter of the aggregate (in our case $h(r_0, \xi) = \exp[-r_0/\xi]$) [42].

The scattered intensity $I(q)$ from a collection of particles can be described by: $I(q) \propto P(q)S(q) + C_{BKG}$. Where $S(q)$ is the structure factor and $P(q)$ is the form factor which describes the scattered intensity function for single primary magnetic nanoparticles. C_{BKG} is added in order to take into account the incoherent background, from the fit was found a constant dependency of C_{BKG} with the momentum transfer vector q. In this paper we use a form factor for polydisperse spheres with mean radius size r_0, which is given by $P(q) = \int_0^\infty K^2(q, r_0, \Delta\eta) f(r_0) \mathrm{d}r_0$, when $\Delta\eta$ is the scattering length density difference between magnetic nanoparticles and the matrix

and $K = \frac{4}{3}\pi r_0^3 \Delta\eta^3 \sin(qr_0) - qr_0\cos(qr_0)/(qr_0)^3$. In previous expression, we assume a lognormal particle size distribution, $f(r_0)$, in order to take into account the polydisperse nature of the ferrofluid used in the synthesis of the magnetic MNCPs.

Fig. 6 shows the fit curves (see continuous red line). As can be observed, fitting curves are in good agreement with the experimentally collected data. For fitting purposes, the parameters C_{BKG}, D_F, and ξ were taken as free variables. Regarding to r_0, it was fitted first in $P(q)$, then, the obtained value was fixed in the structure factor expression, *i.e.* we assume that the aggregates are constituted by primary particles of mean radius r_0. Fitting parameters obtained are summarized Table 2.

The average particle diameters, estimated from the position of the maximum ($2r_0$), are 8.6 nm, 8.9 and 8.0 nm for samples M_1, M_2 and M_3, respectively. These values correlate well with the diameters of the magnetic nanoparticles calculated from TEM (TEM images are available in reference [12]). Despite that the magnetic nanoparticles come from the same ferrofluid, there are noticeable differences in D_{SAXS} values. Such differences can be explained from the interference among neighboring iron oxide particles [38,43]. Clearly, the inter-particle interference effect occurs in different ways depending on the sample. In addition, it is worth noting that in low-q region the slope of the linear part is greater in sample M_3 than in the other samples (see Fig. 6). Then, greater interference effects are present in sample M_3. Previous results are supported with ξ and D_F obtained values. Maximum aggregates sizes are indicating the formation of larger aggregates in sample M_3 with $\xi \approx 99$ nm, while in samples M_1 and M_2 aggregate sizes of $\xi \approx 73$ nm and 25 nm were obtained, respectively. Regarding to D_F values, fractal exponent remains almost constant with values between 1 and 2, indicating that the aggregates keep a branched structure [44], rather well defined in all samples. However, it is observed that the fractal dimension obtained for sample M_3 ($D_F = 1.58$) is slightly higher than those obtained for the others two samples ($D_F = 1.36$ and 1.39 for samples M_1 and M_2, respectively), which could indicate a slightly more compact structure in it. According to the above information (shortest distance among nanoparticles that are forming aggregates and bigger aggregates), it can be inferred that in sample M_3, the magnetic interactions between nanoparticles are more relevant than in others two samples (as shown in the following sections).

3.6. Magnetic properties

The magnetic properties of the MNCPs were analyzed by ZFC-FC and magnetization vs. field measurements. As already mentioned, the magnetic properties of the three systems studied here shall be compared with the results of sample M_X. Magnetic results were employed to study how the nanoparticle aggregation (which is directly related to the magnetic interaction strength among magnetite nanoparticles) affects or distorts the magnetic properties of the MNCPs while it is kept a constant concentration of magnetite nanoparticles.

Fig. 7 shows the ZFC-FC results. In a first approximation the experimental curves of samples M_X, M_1 and M_2 are typical of superparamagnetic particles whose grain sizes are within the single domain limit. On the other hand, the shape of the corresponding curve for sample M_3 presents a wider peak shifted towards higher temperatures. For this sample, it is also possible to see a flat behavior in the FC curve. These trends are distinctive behaviors of systems formed by interacting, not percolated, magnetic nanoparticles. From these data, the blocking temperature (T_B) was determined (corresponding approximately to the maximum of the ZFC curve), being 70 K, 77 K, 87 K and 128 K for M_X, M_1, M_2 and M_3, respectively. From Fig. 7, the splitting points between ZFC and FC curves as well as the maximum of the ZFC curves shift to higher temperatures, indicate an increase in the effective energy barrier [45]. This behavior can be explained by an increase in the dipolar interactions. Usually, an increase in dipolar interactions are attributed to the increase in nanoparticle concentration [46], also related to wider polydispersity or bigger magnetic nanoparticle sizes [47]. Since in our case the nanoparticle concentration (1 wt.%), polydispersity and mean nanoparticle size were kept constant, we attribute the increase in the dipolar interactions to the nanoparticle arrangement in the bio-based matrices. These results are in good agreement with TGA, DMA and SAXS results, which suggest a preferential interaction of oleic acid coated-MNPs with TO bio-

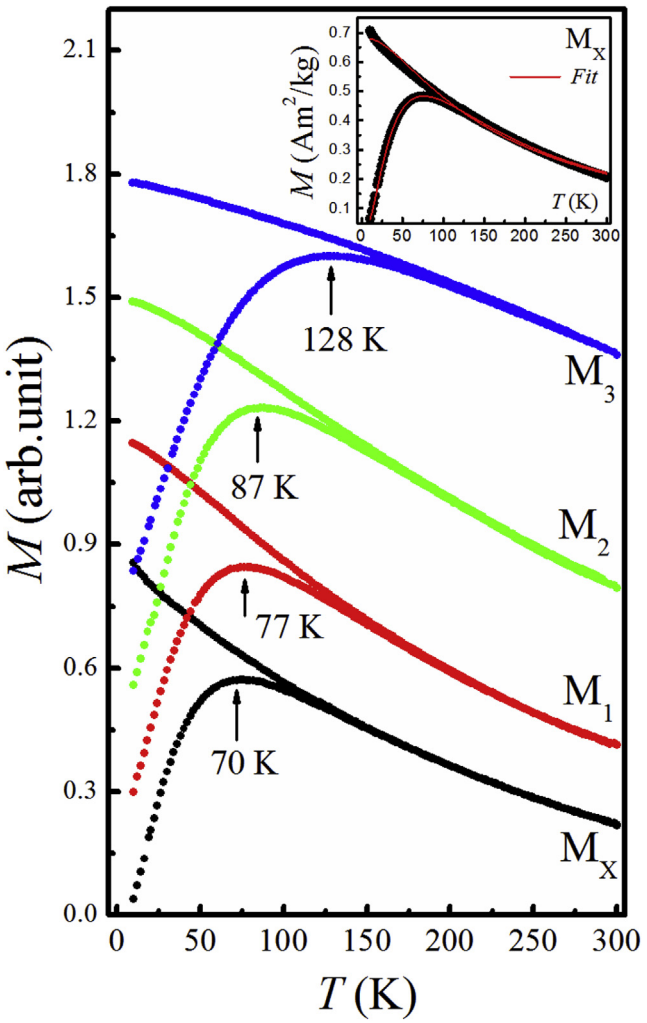

Fig. 7. ZFC-FC measurements of all samples, under a magnetic field of 4 kA/m. Inset: ZFC-FC experimental data (black symbols) of sample M_X and fitting curve (full red line) by equations (2) and (3).

Table 2
SAXS fitted parameters. Constant background C_{BKG}, cluster size ξ, fractal dimension D_F, standard deviation of the lognormal size distributions σ. Mean size was calculated using $D_{SAXS} = 2r_0 exp(\sigma^2/2)$.

Sample	C_{BKG} (10^{-4})	ξ (nm)	D_F	σ	D_{SAXS} (nm)
M_1	2.3	24.5	1.39	0.36	8.6
M_2	2.4	72.9	1.36	0.31	8.9
M_3	4.1	99.5	1.58	0.38	8.0

comonomer.

In non-interacting systems, Néel theory is commonly used to estimate the magnetic anisotropy constant K_{eff}. This constant, called effective anisotropy, includes contributions from magnetocrystalline (bulk), shape, strain, and surfaces anisotropies [48,49]. Then, the determination of T_B allows an estimation of K_{eff} using the classical formula $K_{eff} = 25k_BT_B/V$, where k_B is the Boltzmann constant and V the average volume of magnetic nanoparticles. In the calculations, the volume was determined based on a mean diameter of 9 nm according to previous results [12] and SAXS investigations. Then, K_{eff} values obtained were: 6.3×10^4 J/m^3, 6.9×10^4 J/m^3, 7.9×10^4 J/m^3, and 1.2×10^5 J/m^3 for samples M_X, M_1, M_2 and M_3, respectively. Although the first three values are in the same order of magnitude that those reported in the literature for similar systems [46,50,51], one can observe some differences in that value (and therefore in the energy barrier E_B), which is not expected since the MNPs used to synthesize all MNCPs come from the same ferrofluid. Thus, it is clear that the effective energy barrier E_B is poorly estimated (especially in samples with higher blocked temperatures), and must be corrected taking into account the interparticle interactions.

The K_{eff} value obtained from sample M_X, which has weaker interparticle interactions ($K_{eff} = 6.3 \times 10^4$ J/m^3 and $E_B = 2.4 \times 10^{-20}$ J) is assumed to be the closest to the real value. This hypothesis is based on the fact that the ZFC curve of this sample has the lowest T_B value as well as that, the FC curve does not reach a plateau as soon as T_B is reached. Therefore, we decided to fit the ZFC-FC data of this sample using the superparamagnetic classical equations presented by Hansen and Mørup [52] and by Knobel et al. [45]. Briefly, in their work, the authors follow the framework of the superparamagnetic model, in which the initial susceptibility (M/H, with H much smaller than the anisotropy field) for a single particle size in superparamagnetic regime is given by $\chi_{SPM} = \mu_0 M_S^2 V/3k_BT$ for $T > T_B$ and in blocked regime $\chi_{BL} = \mu_0 M_S^2/3K_{eff}$ for $T < T_B$; μ_0 being the vacuum permeability. Then, they established that the magnetic ZFC susceptibility (M_{ZFC}/H) of a system of polydispersed magnetic nanoparticles with a distribution of reduced energy barriers $f(y)$ with $y = E_B/E_{BM}$ being E_{BM} the median energy barrier, is given by:

$$\frac{M_{ZFC}}{H} = \frac{\mu_0 M_S^2}{3K_{eff}} \left[\frac{E_{BM}}{k_B} \int_0^{T/T_{BM}} T^{-1}\, y f(y) \mathrm{d}y + \int_{T/T_{BM}}^{\infty} f(y) \mathrm{d}y \right] \quad (2)$$

Where $T_{BM} = E_{BM}/k_B ln(\tau_m/\tau_0)$. In eq. (2) the first term corresponds to the contribution of superparamagnetic nanoparticles and the second one corresponds to contributions from blocked magnetic nanoparticles. Regarding to FC curve, it is assumed that the contribution from blocked (below T_B) magnetic nanoparticles to the magnetization is not randomly oriented. In this case the FC susceptibility (M_{FC}/H) is

$$\frac{M_{FC}}{H} = \frac{\mu_0 M_S^2}{3K_{eff}} \frac{E_{BM}}{k_B} \left[\int_0^{T/T_{BM}} T^{-1} y f(y) \mathrm{d}y + \int_{T/T_{BM}}^{\infty} T_B(yE_{BM}) f(y) \mathrm{d}y \right] \quad (3)$$

In addition, in eq. (3), the first contribution is from superparamagnetic nanoparticles, while the second one is from blocked magnetic nanoparticles [45,52]. We considered $f(y)$ as a log-normal distribution, defined as $f(y) = N/\sqrt{2\pi} y\sigma \exp(-\ln^2 y/2\sigma^2)$ being σ the standard deviation. For illustration purposes, the inset of Fig. 7 shows the fit of the experimental curve of the sample M_X (red continuous line). Taking H and τ_m as fixed values (4 kA/m and 100 s respectively), the fit leads to $K_{eff} = 5.53 \times 10^4$ J/m^3 and $\tau_0 = 4.1 \times 10^{-10}$ s, respectively. Under this perspective, one can say that the K_{eff} value is in good agreement with that calculated from the classical equation (K_{eff}=$25k_BT_B/V$). The obtained τ_0 value is in good agreement with the theoretical one, which according to the Néel theory is in the range 10^{-11} s to 10^{-9} s for superparamagnetic nanoparticles. Therefore, these results confirm the non-interacting nature of MNPs in sample M_X. Based on this, we can consider this system closer to an ideal superparamagnet than the others and thus, as a reference on the magnetic properties interpretations.

Magnetizations vs. field measurements were carried out for every sample at various temperatures. Fig. 8 shows the reduced magnetization plotted as a function of M_S (H/T) and H/T, usually known as superparamagnetic scaling laws. These laws are used to test whether the magnetization process, of a sample measured at various temperatures, is influenced by dipolar interactions. If the particles are in non-interacting superparamagnetic regime (SPM), the curves (related to each temperature) must overlap in a scaling law M/MS vs. $M_S(H/T)$ for $T < T_B$ or in M/M_S vs. H/T for $T > T_B$ [27,45,53,54].

Table 3 summarizes the coercive field (H_C) and saturation magnetization (M_S) values determined from M vs. H curves. In all samples, the coercive values are close to zero for $T < T_B$ and tend to higher values as temperature decrease. Such values are consistent with ZFC and FC results.

In our case, we wanted to analyze the effect of dispersion and dipolar interactions in MNCPs. To achieve this task, we plotted the experimental $M(H)$ data of each sample at a fixed temperature (300 K). This procedure was done knowing that: (*i*) our samples have the same nanoparticle concentrations (1 wt.%), (*ii*) they come from the same synthesis procedure and, (*iii*) when the M_S values are compared, at a fixed temperature, different values were obtained (see Table 3). Then, if the magnetic nanoparticles would have the same random arrangement, one would obtain a single overlapped curve when the *M vs. H* data of each sample would be plotted at a fixed temperature. However, such behavior was not observed in our systems (see Fig. 8 *a* and *b*) confirming that the inter-particle interactions effects are different in each sample. This also indicates, in a slightly indirect way, that composition matrix affects the spatial distribution of the MNPs. Better proximity between curves is observed in Fig. 8 *b* possibly indicating that at $T = 300$ K magnetite nanoparticles are in the unblocked regime.

To gain a deeper understanding on the role of magnetic interactions in our systems, a more quantitative analysis was then performed. First, we used the standard Langevin equation, weighted with a log-normal moment distribution, to fit the M vs. H experimental data. Therefore, the magnetization contribution of the unblocked MNP nanoparticles, $M(H,T)$, is described by [45].

$$M(H,T) = \int_0^{\infty} \mu_{AP} L[\mu_0 \mu_{AP} H/k_B T] f(\mu_{AP}) \mathrm{d}\mu_{AP} \quad (4)$$

Where $L[\mu_0\mu_{AP}H/k_BT]$ is the Langevin function, μ_{AP} is the *apparent* magnetic moment (named *apparent* since the previous equation does not take into account possible inter-particle interactions) and $f(\mu_{AP})$ represents the lognormal distribution of the *apparent* magnetic moments. Fit results are graphically presented in Fig. 8 *a* (for comparative purposes were plotted following the scaling laws). From the fit, we could determine the median of the lognormal magnetic moment distribution (x_0) and its standard deviation (σ), the *apparent* number of magnetic nanoparticles per volume unit (N_{AP}) and, the mean of the *apparent* magnetic moments (μ_{AP}) (estimated from $\mu_{AP} = x_0\, exp[\sigma^2/2]$). These values are summarized in Table 4.

Fig. 9 presents the temperature behavior of the *apparent*

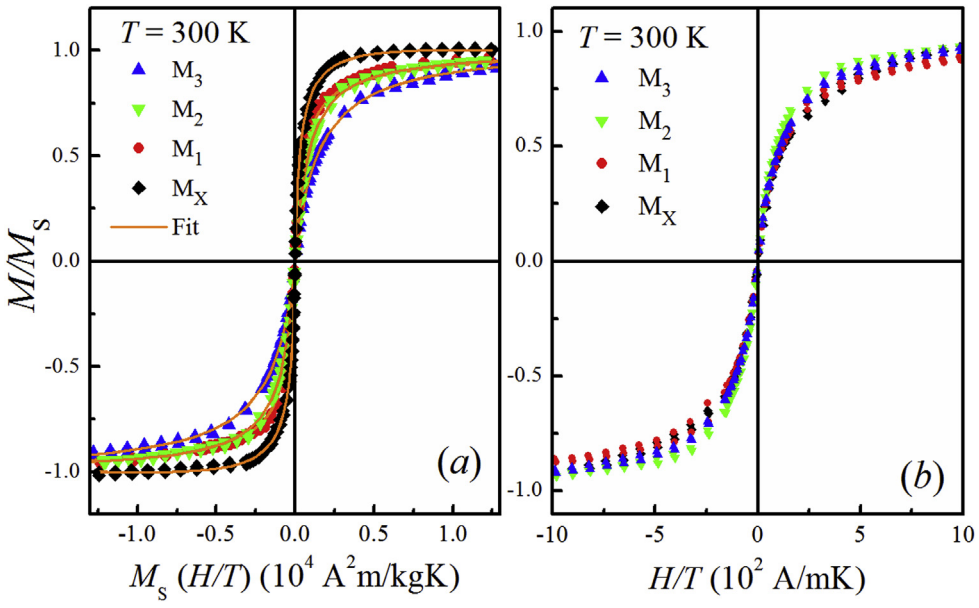

Fig. 8. Reduced magnetization as a function of M_S (H/T) and H/T for samples M_X, M_1, M_2 and M_3.

Table 3
Best fitting parameter values obtained for M vs. H experimental curves. Calculated from Equation (4). Mean of the apparent magnetic moments μ_{AP} values were estimated from $\mu_{AP} = x_0\, exp[\sigma^2/2]$.

	Mx			M_1			M_2			M_3		
T (K)	N_{AP} (10^{22} m^{-3})	σ	μ_{AP} (10^3 μ_B)	N_{AP} (10^{22} m^{-3})	σ	μ_{AP} (10^3 μ_B)	N_{AP} (10^{22} m^{-3})	Σ	μ_{AP} (10^3 μ_B)	N_{AP} (10^{22} m^{-3})	σ	μ_{AP} (10^3 μ_B)
70	7.06	1.08	4.11	9.89	1.33	2.92	30.38	3.03	4.05	52.89	0.92	52.20
120	4.11	1.08	6.82	9.70	1.18	5.76	16.53	1.07	7.18	31.14	0.98	49.95
200	2.85	1.02	9.53	5.40	1.01	9.75	9.96	0.98	11.11	19.82	1.00	44.62
250	3.20	1.10	8.46	5.03	1.04	10.10	6.69	0.84	15.51	15.85	0.99	41.59
300	3.99	1.16	6.87	3.80	0.93	12.47	5.63	0.78	17.42	11.50	0.92	41.66

Table 4
Corrected parameter obtained from ISP equations: $\mu_{AP} = 1/1 + T^*/T\mu_{CO}$ and $N_{AP} = (1 + T^*/T)N_{CO}$.

	Mx		M_1		M_2		M_3	
T (K)	N_{CO} (10^{22} m^{-3})	μ_{CO} (10^3 μ_B)	N_{CO} (10^{22} m^{-3})	μ_{CO} (10^3 μ_B)	N_{CO} (10^{22} m^{-3})	μ_{CO} (10^3 μ_B)	N_{CO} (10^{22} m^{-3})	μ_{CO}.(10^3 μ_B)
70	3.33	8.72	1.93	14.96	3.45	35.69	3.34	52.20
120	2.54	11.03	2.98	18.73	3.11	38.12	3.40	49.95
200	2.15	12.61	2.39	22.03	2.96	37.30	3.67	44.62
250	2.60	10.43	2.61	19.48	2.53	40.89	3.73	41.59
300	3.37	8.13	2.19	21.63	2.50	39.24	3.40	41.66

magnetic moment (black symbols). The obtained values increase with the temperature, which is an unrealistic behavior (observed in other systems [55]). The expected behavior of μ_{AP} is almost constant for low temperatures and decrease as the temperature approaches the Curie temperature (analogously to the $M_S(T)$ behavior). In order to obtain the proper dependence of the magnetic moment, Allia et al. proposed the so-called *Interacting Superparamagnetic Model* (ISP) [27]. Such model describes the behavior of the anhysteretic magnetization curves affected by a weak, but non negligible, dipolar interaction. This model has been successfully used on a variety of weakly interacting nanoparticle systems [27,45,53,56–60]. Briefly, the existence of a dipolar field, which acts by altering in a random way the magnetic moments, their directions, sign, and magnitude. This effect is analogous to the effect produced by the temperature, such that the temperature in the Langevin function can be written as $T_A = T + T^*$, when T^* is related to the dipolar energy ($\varepsilon_D = k_B T^*$). Accordingly, the magnetization is described by a modified Langevin function.

$$M(H,T) = \int_0^\infty \mu_{CO} L[\mu_0 \mu_{CO} H/k_B(T+T^*)] f(\mu_{CO}) d\mu_{CO} \quad (5)$$

According to the ISP model, the only required parameter to calculate the *corrected* magnetic moment (μ_{CO}), from μ_{AP}, is T^*, which is directly obtained through the ISP analysis (procedure for calculating that temperature is described in [27]). Through ISP model the following relations are established.

$$\langle \mu_{AP} \rangle = \frac{1}{1 + T^*/T} \langle \mu_{CO} \rangle \text{ and } N_{AP} = \left(\frac{1+T^*}{T}\right) N_{CO}. \quad (6)$$

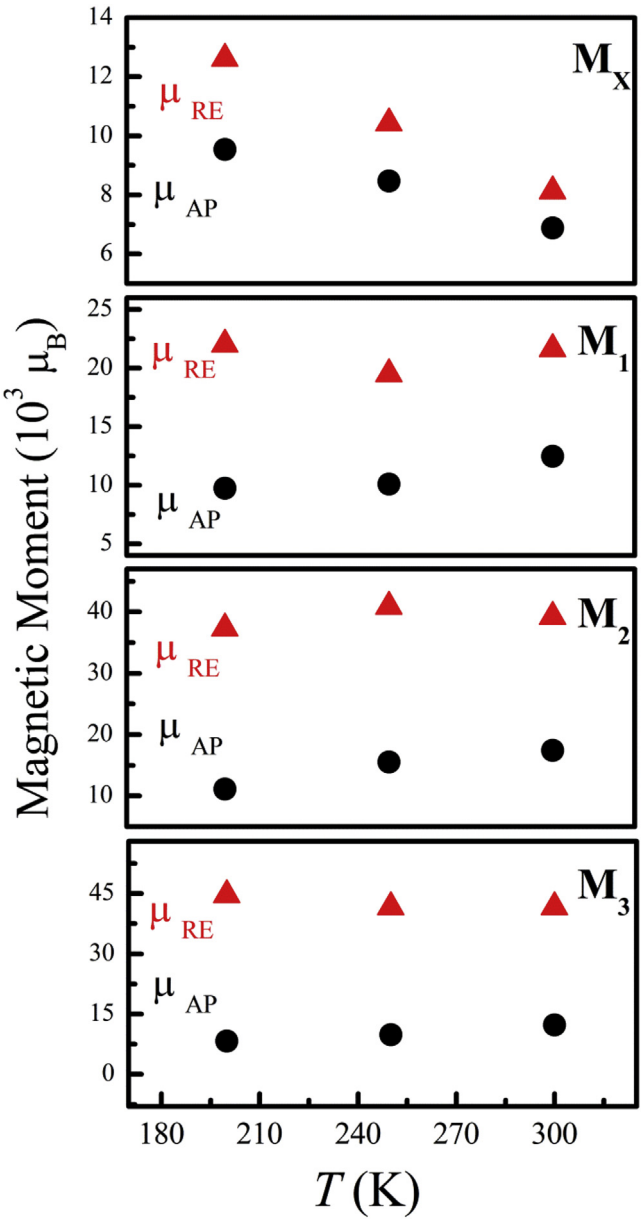

Fig. 9. Real and apparent mean magnetic moment values as function of temperature for all samples. Symbols represent the values obtained from the fit using Equation (5).

The magnetic moment was calculated with eq. (6), and the obtained values are summarized in Table 4.

Fig. 9 shows the temperature behavior of the *corrected* magnetic moment (red symbols). Sample M_3 (more interacting sample) display higher values of μ_{CO}, when compared to the corresponding values of the other samples, and its behavior as function of T is almost constant. Magnetic moments of the M_3 sample are higher than the expected ones for these sizes of magnetic nanoparticles. Since this sample is also the one with more interacting particles, it could be possible that the model considers a group of magnetic nanoparticles that coherently rotates with a unique effective magnetic moment. It is also remarkable that the difference $\mu_{CO}-\mu_{AP}$ increases as the magnetic interactions rise, being notable that for samples M_1, M_2 and M_3, when the μ_{CO} values are around one order of magnitude higher than the corresponding μ_{AP} values. All these characteristics are related to the magnitude of the interparticle magnetic interactions, such that the more interacting samples are far from the ISP model, and more complex magnetization processes are taking place.

On the other hand, for samples M_1 and M_X, the corrected magnetic moment, for $T \geq 150$ K, has values close to the expected ones. It is worth mentioning that in the samples with weaker magnetic interactions and with more dispersed magnetic nanoparticles (M_X and M_1) the ISP model successfully describes the magnetic response of these systems for $T > 200$ K. It is also remarkable that the μ_{CO} value of sample M_X at $T = 300$ K is in very good agreement with those reported for similar systems [56,57,60].

4. Conclusions

Physicochemical properties of novel synthesized ultra-diluted green nanocomposites, based on a vegetable oil and 1wt.% of magnetite nanoparticles coated with oleic acid, were studied.

The glass transition temperature (Tg) of the three nanocomposites increased due to incorporation of 1wt.% of MNP as a consequence of the different relaxation mechanisms and inhomogeneities that appeared in the materials because of the presence of the magnetic nanoparticles. The storage modulus and mechanical properties were also modified by the presence of the magnetic nanoparticles. All MNCPs maintained good damping properties over a range of materials wider than unfilled materials. The MNPs did not behave as inert fillers in the nanocomposites studied. Instead, they affected the structure of the polymer network and the spatial arrangement of MNPs inside the matrices. The morphology of the nanocomposites allowed showing that MNCPs presents different degree of MNP dispersion and aggregation.

Furthermore, the nanocomposites presented typical magnetic behavior of interacting superparamagnetic particles, whose grain sizes are within the single domain limit. From magnetic properties, significant differences in the magnetic behavior are observed as consequence of magnetic interactions among nanoparticles and the formation of aggregates. These last facts were corroborated by SAXS. Hence, in this work we could demonstrate that keeping constant the magnetic nanoparticles concentration, magnetic interparticle interactions increases only by the different chemical affinities between oleic acid and the different components of the biobased matrices.

Acknowledgments

The work at UNICAMP was supported by FAPESP (2011/01235-6, 2011/02356-11, and 2014/26672-8) and CNPq (506394/2013-1) Brazil. Small-angle X-ray scattering data were acquired at beamline D11A-SAXS1 (17036), D11A-SAXS2 (14355) at LNLS (Campinas, SP, Brazil) and SEM images (17596) were taken at the LNNano of National Nanotechnology Laboratory (CNPEM, Campinas, Brazil). The authors thanks M. E. F. Brollo for help during the SAXS acquisitions and Cooperativa Agrícola de Picada Libertad for the supply of tung oil, the financial support of CONICET, UNMdP and ANPCyT from Argentina.

References

[1] M. Darder, P. Aranda, E. Ruiz-Hitzky, Bionanocomposites: a new concept of ecological, bioinspired, and functional hybrid materials, Adv. Mater 19 (2007) 1309–31319.
[2] V. Mittal, Nanocomposites with Biodegradable Polymers: Synthesis, Properties, and Future Perspectives, Oxford University Press, 2011.
[3] N.D.G. Souza, R.M. Freire, A.P. Cunha, M.A.S. da Silva, S.E. Mazzetto, A.S.B. Sombra, J.C. Denardin, N.M.P.S. Ricardo, P.B.A. Fechine, New magnetic nanobiocomposite based in galactomannan/glycerol and superparamagnetic nanoparticles, Mater. Chem. Phys. 156 (2015) 113–120.
[4] S.C. McBain, H.H.P. Yiu, J. Dobson, Magnetic nanoparticles for gene and drug delivery, Int. J. Nanomedicine 3 (2008) 169–180.

[5] R. Sensenig, Y. Sapir, C. MacDonald, S. Cohen, B. Polyak, Magnetic nanoparticle-based approaches to locally target therapy and enhance tissue regeneration in vivo, Nanomedicine 7 (2012) 1425–1442.
[6] A.S. Wahajuddin, Superparamagnetic iron oxide nanoparticles: magnetic nanoplatforms as drug carriers, Int. J. Nanomed. 7 (2012) 3445–3471.
[7] N. Karak, Vegetable Oil-based Polymers, Elsevier, 2012.
[8] G. Lligadas, J.C. Ronda, M. Galià, V. Cádiz, Renewable polymeric materials from vegetable oils: a perspective, Mater. Today 16 (2013) 337–343.
[9] L. Yu, K. Dean, L. Li, Polymer blends and composites from renewable resources, Prog. Polym. Sci. 31 (2006) 576–602.
[10] I. Armentano, M. Dottori, E. Fortunati, S. Mattioli, J.M. Kenny, Biodegradable polymer matrix nanocomposites for tissue engineering: a review, Polym. Degrad. Stab. 95 (2010) 2126–2546.
[11] S. Kirchberg, M. Rudolph, G. Ziegmann, U.A. Peuker, Nanocomposites based on technical polymers and sterically functionalized soft magnetic magnetite nanoparticles: synthesis, processing, and characterization, J. Nanomater (2012) 1–8.
[12] C. Meiorin, D. Muraca, K.R. Pirota, M.I. Aranguren, M.A. Mosiewicki, Nanocomposites with superparamagnetic behavior based on a vegetable oil and magnetite nanoparticles, Eur. Polym. J. 53 (2014) 90–99.
[13] E.U.X. Péres, F.G. de Souza, F.M. Silva, J.A. Chaker, P.A.Z. Suarez, Biopolyester from ricinoleic acid: synthesis, characterization and its use as biopolymeric matrix for magnetic nanocomposites, Ind. Crop. Prod. 59 (2014) 260–267.
[14] R. Hergt, S. Dutz, R. Müller, M. Zeisberger, Magnetic particle hyperthermia: nanoparticle magnetism and materials development for cancer therapy, J. Phys. Condens. Matter 18 (2006) S2919–S2934.
[15] J. Leng, X. Lan, Y. Liu, S. Du, Shape-memory polymers and their composites: stimulus methods and applications, Prog. Mater. Sci. 56 (2011) 1077–1135.
[16] P.R. Buckley, Actuation of Shape Memory Polymer Using Magnetic Fields for Applications in Medical Devices, 2004.
[17] D. Serantes, K. Simeonidis, M. Angelakeris, O. Chubykalo-Fesenko, M. Marciello, M.P. Morales, D. Baldomirm, C. Martinez-Boubeta, Multiplying magnetic hyperthermia response by nanoparticle assembling, J. Phys. Chem. C 118 (2014) 5927–5934.
[18] M.E. De Sousa, M.B. Fernández van Raap, P.C. Rivas, P. Mendoza Zélis, P. Girardin, G.A. Pasquevich, J.L. Alessandrini, D. Muraca, F.H. Sánchez, Stability and relaxation mechanisms of citric acid coated magnetite nanoparticles for magnetic hyperthermia, J. Phys. Chem. C 117 (2013), 5436–5345.
[19] J.L. O'Dell, IV Internat Conf Woodfiber-plast Compos, Madison, WI, May 12-14, 1997.
[20] J. Thévenot, H. Oliveira, O. Sandre, S. Lecommandoux, Magnetic responsive polymer composite materials, Chem. Soc. Rev. 42 (2013) 7099–7116.
[21] M. González, I. Martín-Fabiani, J. Baselga, J. Pozuelo, Magnetic nanocomposites based on hydrogenated epoxy resin, Mater. Chem. Phys. 132 (2012) 618–624.
[22] D.F. Coral, P. Mendoza Zélis, M.E. de Sousa, D. Muraca, V. Lassalle, P. Nicolás, M.L. Ferreira, M.B. Fernández van Raap, Quasi-static magnetic measurements to predict specific absorption rates in magnetic fluid hyperthermia experiments, J. Appl. Phys. 115 (2014) 043907.
[23] G. Salas, J. Camarero, D. Cabrera, H. Takacs, M. Varela, R. Ludwig, H. Dahring, I. Hilger, R. Miranda, M.P. Morales, F.J. Teran, Modulation of magnetic heating via dipolar magnetic interactions in monodisperse and crystalline iron oxide Nanoparticles, J. Phys. Chem. C 118 (2014) 19985–19994.
[24] Luis C. Branquinho, Marcus S. Carrião, S. Anderson, Nicholas Zufelato Costa, Marcelo H. Sousa, Ronei Miotto, Robert Ivkov, Andris F. Bakuzis, Effect of magnetic dipolar interactions on nanoparticle heating efficiency: Implications for cancer hyperthermia, Sci. Rep. 3 (2013) 2887.
[25] I.S. Smolkova, N.E. Kazantseva, Harshida Parmar, Vladimir Babayan, P. Smolka, P. Saha, Correlation between coprecipitation reaction course and magneto-structural properties of iron oxide nanoparticles, Mater. Chem. Phys. 155 (2015) 178–190.
[26] C. Meiorin, M.I. Aranguren, M.A. Mosiewicki, Polymeric networks based on tung oil: reaction and modification with green oil monomers, Eur. Polym. J. 67 (2015) 551–560.
[27] P. Allia, M. Coisson, P. Tiberto, F. Vinai, M. Knobel, M. Novak, et al., Granular Cu-Co alloys as interacting superparamagnets, Phys. Rev. B 64 (2001) 144420.
[28] R. Massart, R.,V. Cabuil, Synthesis of colloidal magnetite in alkaline medium: yield and particle size control, J.Chim. Phys. 84 (1987) 967–973.
[29] C. Meiorin, M.I.A. Mosiewicki, M.I. Aranguren, M.A. Mosiewicki, Vegetable oil based thermoset copolymers with shape memory behavior and damping capacity, Polym. Int. 64 (2012) 735–742.
[30] C. Meiorin, M.I. Aranguren, M.A. Mosiewicki, Smart and structural thermosets from the cationic copolymerization of a vegetable oil, J. Appl. Polym. Sci. 124 (2012) 5071–5078.
[31] L. Benavides Rodríguez, M.R. Sibaja Ballesteros, J.R. Vega-Baudrit, M. Camacho Elizondo, S. Madrigal-Carball, Estudio cinético de la degradación térmica de quitina y quitosano de camarón de la especie “Heterocarpus vicarius” empleando la técnica termogravimétrica en modo dinámico, Rev. Iberoam. Polímeros 11 (2010) 558–573.
[32] V. Belessi, R. Zboril, J. Tucek, M. Mashlan, V. Tzitzios, D. Petridis, Ferrofluids from magnetic-chitosan hybrids, Chem. Mater 20 (2008) 3298–3305.
[33] G.A. Kloster, M.E. Marcovich, M.A. Mosiewicki, Composite films based on chitosan and nanomagnetite, Eur. Polym. J. 66 (2015) 386–396.
[34] D. Hritcu, M.I. Popa, N. Popa, V. Badescu, V. Balan, Preparation and characterization of magnetic chitosan nanospheres, Turk. J. Chem. 33 (2009) 785–796.
[35] F. Li, J. Hasjim, R.C. Larock, Synthesis, structure, and thermophysical and mechanical properties of new polymers prepared by the cationic copolymerization of corn oil, styrene, and divinylbenzene, J. Appl. Polym. Sci. 90 (2003) 1830–1838.
[36] M.A. Mosiewicki, J. Borrajo, M.I. Aranguren, Mechanical properties of wood-flour/linseed oil resin composites, Polym. Int. 54 (2005) 829–836.
[37] M.A. Mosiewicki, U. Casado, N.E. Marcovich, M.I. Aranguren, Polyurethanes from tung oil: polymer characterization and composites, Polym. Eng. Sci. 49 (2009) 685–692.
[38] A.V. Teixeira, I. Morfin, F. Ehrburger-Dolle, C. Rochas, P. Panine, P. Licinio, et al., Structure and magnetic properties of dilute ferrofluids suspended in gels, Compos. Sci. Technol. 63 (2003) 1105–1111.
[39] M.B. Fernández van Raap, P. Mendoza Zélis, D.F. Coral, T.E. Torres, C. Marquina, G.F. Goya, et al., Self organization in oleic acid-coated $CoFe_2O_4$ colloids: a SAXS study, J. Nanoparticle. Res. 14 (2012) 1072.
[40] A. Millan, F. Palacio, A. Falqui, E. Snoeck, V. Serin, A. Bhattacharjee, et al., Maghemite polymer nanocomposites with modulated magnetic properties, Acta. Mater 55 (2007) 2201–2209.
[41] S.-H. Chen, J. Teixeira, Structure and fractal dimension of protein-detergent complexes, Phys. Rev. Lett. 57 (1986) 2583–2586.
[42] SASfit: Small Angle Scattering (SAS) Data Analysis Software for Fitting Simple Form Factors and Structure Factors. https://kur.web.psi.ch/sans1/SANSSoft/sasfit.html (accessed May 14, 2015).
[43] E.V. Shtykova, X. Huang, N. Remmes, D. Baxter, B. Stein, B. Dragnea, et al., Structure and properties of iron oxide nanoparticles encapsulated by phospholipids with poly(ethylene glycol) tails, J. Phys. Chem. C 111 (2007) 18078–18086.
[44] J.M.J. Santillán, M.B. Fernández van Raap, P. Mendoza Zélis, D. Coral, D. Muraca, D.C. Schinca, et al., Ag nanoparticles formed by femtosecond pulse laser ablation in water: self-assembled fractal structures, J. Nanoparticle. Res. 17 (2015) 86.
[45] M. Knobel, W.C. Nunes, L.M. Socolovsky, E. De Biasi, J.M. Vargas, J.C. Denardin, Superparamagnetism and other magnetic features in granular materials: a review on ideal and real systems, J. Nanosci. Nanotechnol. 8 (2008) 2836–2857.
[46] O. Moscoso-Londoño, J.S. Gonzalez, D. Muraca, C.E. Hoppe, V.A. Alvarez, A. López-Quintela, et al., Structural and magnetic behavior of ferrogels obtained by freezing thawing of polyvinyl alcohol/poly(acrylic acid) (PAA)-coated iron oxide nanoparticles, Eur. Polym. J. 49 (2013) 279–289.
[47] A. Demortière, P. Panissod, B.P. Pichon, G. Pourroy, D. Guillon, B. Donnio, et al., Size-dependent properties of magnetic iron oxide nanocrystals, Nanoscale 3 (2011) 225–232.
[48] K. Nawara, J. Romiszewski, K. Kijewska, J. Szczytko, A. Twardowski, M. Mazur, et al., Adsorption of doxorubicin onto citrate-stabilized magnetic nanoparticles, J. Phys. Chem. C 116 (2012) 5598–5609.
[49] Y. Komorida, M. Mito, H. Deguchi, S. Takagi, A. Millan, N.J.O. Silva, et al., Surface and core magnetic anisotropy in maghemite nanoparticles determined by pressure experiments, Appl. Phys. Lett. 94 (2009) 202503.
[50] G.F. Goya, T.S. Berquo, F.C. Fonseca, M.P. Morales, Static and dynamic magnetic properties of spherical magnetite nanoparticles, J. Appl. Phys. 94 (2003) 3520.
[51] S.Y. Lee, J.S. Lee, B.K. Kim, Preparation and properties of water-borne polyurethanes, Polym. Int. 42 (1997) 67–76.
[52] M.F. Hansen, S. . Mørup, Estimation of blocking temperatures from ZFC/FC curves, J. Magn. Magn. Mater 203 (1999) 214–216.
[53] P. Allia, P. Tiberto, Dynamic effects of dipolar interactions on the magnetic behavior of magnetite nanoparticles, J. Nanoparticle. Res. 13 (2011) 7277–7293.
[54] A. Tamion, M. Hillenkamp, F. Tournus, E. Bonet, V. Dupuis, Accurate determination of the magnetic anisotropy in cluster-assembled nanostructures, Appl. Phys. Lett. 95 (2009) 062503.
[55] M. Knobel, W.C. Nunes, A.L. Brandl, J.M. Vargas, L.M. Socolovsky, D. Zanchet, Interaction effects in magnetic granular systems, Phys. B. Condens. Matter 354 (2004) 80–87.
[56] J.M. Vargas, W.C. Nunes, L.M. Socolovsky, M. Knobel, D. Zanchet, Effect of dipolar interaction observed in iron-based nanoparticles, Phys. Rev. B 72 (2005) 184428.
[57] P. Mendoza Zélis, D. Muraca, J.S. Gonzalez, G.A. Pasquevich, V.A. Alvarez, K.R. Pirota, et al., Magnetic properties study of iron-oxide nanoparticles/PVA ferrogels with potential biomedical applications, J. Nanoparticle. Res. 15 (2013) 1613.
[58] O. Moscoso-Londoño, D. Muraca, P. Tancredi, C. Cosio-Castañeda, K.R. Pirota, L.M. Socolovsky, Physicochemical studies of complex silver–magnetite nanoheterodimers with controlled morphology, J. Phys. Chem. C 118 (2014) 13168–13176.
[59] P. Allia, P. Tiberto, M. Coisson, A. Chiolerio, F. Celegato, F. Vinai, et al., Evidence for magnetic interactions among magnetite nanoparticles dispersed in photoreticulated PEGDA-600 matrix, J. Nanoparticle. Res. 13 (2011) 5615–5626.
[60] P. Allia, G. Barrera, P. Tiberto, T. Nardi, Y. Leterrier, M. Sangermano, Fe_3O_4 nanoparticles and nanocomposites with potential application in biomedicine and in communication technologies: nanoparticle aggregation, interaction, and effective magnetic anisotropy, J. Appl. Phys. 116 (2014) 113903.